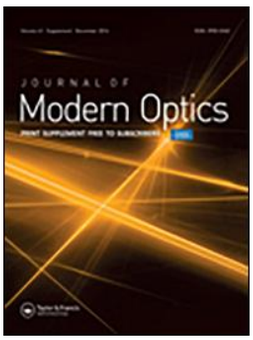

Journal of Modern Optics

ISSN: 0950-0340 (Print) 1362-3044 (Online) Journal homepage: https://www.tandfonline.com/loi/tmop20

# Photodetachment of a model molecular system by an elliptically polarized field

M.V. Frolov, N.L. Manakov, S.S. Marmo & Anthony F. Starace

**To cite this article:** M.V. Frolov, N.L. Manakov, S.S. Marmo & Anthony F. Starace (2015) Photodetachment of a model molecular system by an elliptically polarized field, Journal of Modern Optics, 62:sup2, S21-S33, DOI: 10.1080/09500340.2015.1046522

**To link to this article:** https://doi.org/10.1080/09500340.2015.1046522

© 2015 The Author(s). Published by Taylor & Francis

Published online: 21 Jul 2015.

Submit your article to this journal

Article views: 696

View related articles

View Crossmark data

Citing articles: 1 View citing articles

Full Terms & Conditions of access and use can be found at
https://www.tandfonline.com/action/journalInformation?journalCode=tmop20

*Journal of Modern Optics*, 2015
Vol. 62, No. S2, S21–S33, http://dx.doi.org/10.1080/09500340.2015.1046522

Taylor & Francis
Taylor & Francis Group

# Photodetachment of a model molecular system by an elliptically polarized field

M.V. Frolov[a], N.L. Manakov[a], S.S. Marmo[a] and Anthony F. Starace[b]*

[a]*Department of Physics, Voronezh State University, Voronezh, Russia;* [b]*Department of Physics and Astronomy, The University of Nebraska, Lincoln, NE, USA*

(*Received 25 March 2015; accepted 22 April 2015*)

The differential cross section for one-photon molecular detachment by an elliptically polarized field is analyzed for a one-electron molecular model comprised of an electron in the field of two (generally nonequivalent) attractive zero-range potentials (ZRPs) separated by the distance $R$. A phenomenological parametrization of the photodetachment cross section for a fixed-in-space molecular system in terms of two scalar dynamical parameters is presented and circular dichroism effects are discussed. Analytic results for the dynamical molecular parameters within the ZRP molecular model are used to analyze interference phenomena (including two-center interference) and dichroic effects in the detached electron angular distributions and their dependence on the interatomic distance $R$ and on the orientation of the molecular axis with respect to the polarization plane. Numerical ZRP results for angular distributions are presented for both symmetric and asymmetric molecules in an elliptically polarized field.

**Keywords:** photodetachment; diatomic molecule; elliptical polarization; photoelectron angular distribution; circular dichroism; theoretical model

## 1. Introduction

The great progress of attosecond science in producing short wavelength pulses of attosecond durations represents a major advance for the study of electronic dynamics in atomic and molecular systems [1–4]. In particular, nonlinear attosecond physics holds great promise for both scientific investigations and for technological applications owing to the possibility of studying and using nonlinear effects in a new range of frequencies. At present, however, the intensities of attosecond pulses are sufficiently low that perturbation theory represents an appropriate approach for analyzing their interactions with atoms and molecules. Thus, attosecond pulse photoionization can be described by a transition matrix element given by first-order perturbation theory that is similar to that for photoionization in a monochromatic field [5]. In contrast to photoionization by a monochromatic field, however, the large bandwidth of a very short laser pulse ensures a wide range of ionized electron energies in the final state. This large range of final state photoelectron energies upon ionization by a short attosecond pulse provides an opportunity to observe the interference of the first- and second-order transition amplitudes of perturbation theory in attosecond photoionization of atoms [5]. In photoionization of molecules by attosecond pulses [6–8] as well as by X-rays [9,10], the short wavelength of the radiation has led to novel interference phenomena in the photoelectron angular distributions. For sufficiently short wavelengths, the photoelectron acquires large momentum, making it possible to observe Young-type double-slit interference fringes in the photoionization spectra of molecules [6–10], as proposed by Fano and Cohen [11] and by Kaplan and Markin [12]. More recently [13], this type of interference was observed in partial ionization cross sections, which correspond to the ionization of a molecular electron with a fixed angular momentum in the continuum. These measurements provide access to molecular data that is unavailable in measurements of total (angle-integrated) cross sections, such as, e.g. differences between photoionization of "gerade" and "ungerade" states.

Photoionization cross sections corresponding to the production of photoelectrons with large momenta are necessary also for the control of both laser-induced and laser-assisted strong field processes, such as, e.g. high-order harmonic generation (HHG) and laser-assisted electron recombination and bremsstrahlung processes. This control is based upon the relationship between the photorecombination cross section and that for photoionization by means of the principle of detailed balance. The photorecombination cross section enters the probability of the aforementioned strong field processes as an atomic or molecular factor, which describes the features of the atomic or molecular dynamics in strong field phenomena (see, e.g. Refs. [14–16] for HHG, Refs.

*Corresponding author. Email: astarace1@unl.edu

© 2015 The Author(s). Published by Taylor & Francis.
This is an Open Access article distributed under the terms of the Creative Commons Attribution License (http://creativecommons.org/licenses/by/4.0/), which permits unrestricted use, distribution, and reproduction in any medium, provided the original work is properly cited.

[17,18] for recombination, and Ref. [19] for bremsstrahlung). Based on this factorized dependence of the probability of a strong field process on the target's photorecombination cross section, a new spectroscopic method has been developed: HHG-based spectroscopy of atoms [20,21] and molecules [22–32]. In particular, any occurrence of double-slit interference fringes in the photoionization cross section of a molecule is manifested by corresponding oscillation features in that molecule's HHG spectrum (see, e.g. Refs. [23,28,30]). Many-electron and multichannel dynamical effects in molecular photoionization are also being revealed in molecular HHG spectra [33–39].

Owing to this obvious importance of molecular photoionization cross sections to both attosecond and strong field molecular physics, different theoretical approaches have been developed recently for the calculation of molecular photoionization cross sections. Most are based on numerical solution of the Schrödinger equation [6–8,10,40–45] (see also the recent review [46]), which can provide precise values of cross sections for simple molecular systems. The applications of these methods include calculations of attosecond pulse photoionization of molecules with analyses of the angular and momentum distributions as well as calculations of ordinary one-photon ionization of molecular systems with subsequent analysis of double-slit interference fringes in the momentum distributions. The qualitative description of interference fringes in molecular photoionization spectra is based on the simple picture of the atomic centers of a molecular system as coherent emitters of electronic waves [47]. Within this picture, ionization of an electron (whose initial wave function extends over all molecular centers) by a high-frequency photon results in electronic outgoing waves from all molecular centers. These waves interfere and thereby form interference fringes. Although this picture is oversimplified (since it does not take into account any dynamical effects involving the molecular core), it nevertheless gives reasonable agreement with numerical and experimental results. For nonsymmetric diatomic molecules, however, this "two-emitters" mechanism cannot be employed to describe interference fringes because in this case the electron wave function is mostly localized on one center. Thus the "intensity" of matter waves from one of the two emitters is strongly suppressed with respect to that from the other [9]. The second (less intense) center plays in this case the role of a reflector, i.e. a source of a secondary wave. This secondary wave and the initially emitted spherical wave interfere and exhibit interference fringes [9,48]. These two mechanisms leading to interference fringes cannot be distinguished in numerical simulations, but they are treated explicitly in the two zero-range potential (ZRP) molecular model [48,49].

Owing to the significant dependence of HHG on the driving laser ellipticity, applications of HHG-based spectroscopy have stimulated investigations of photoionization by an elliptically polarized laser field. For this case, in contrast to atomic photoionization, the angular distribution of molecular photoelectrons depends on the sign of the laser ellipticity [42,44]. These dichroic effects in the molecular photoionization are yet not well studied. However, they provide an additional means to control molecular dynamics, since their magnitude is determined by an unusual kind of interference, i.e. that between the real and imaginary (or the Hermitian and non-Hermitian) parts of the photoionization amplitude [50]. Note that such dichroic effects disappear upon averaging the molecular photoionization cross section over the direction of the molecular axis. They also disappear in the plane-wave approximation (in which case the photoionization amplitude is Hermitian). It may be expected that dichroic effects also modify interference phenomena (including two-center interference). However, this problem has apparently never been investigated as far as we are aware.

Clearly, in contrast to the atomic case, both aforementioned specific interference and polarization phenomena in photoionization of a diatomic molecule originate predominantly from the two-center nature of the molecular potential. Thus these phenomena can be qualitatively explained by analyzing the amplitude for molecular photoionization (or photodetachment) for the simplest molecular model, that of an electron bound in the field of two spatially-separated attractive atomic centers subjected to an elliptically polarized, monochromatic (for simplicity) electric field. A more detailed modeling of the atomic center potentials would be required to analyze the role of molecular dynamics on the interference and polarization phenomena that we analyze here.

This paper is organized as follows. In Section 2 we present a general phenomenological parametrization of the amplitude and cross section for one-photon ionization/detachment of a fixed-in-space diatomic molecular system by an elliptically polarized field. This parametrization involves a geometrical factor, given in terms of scalar products of the vectors of the problem, and two scalar dynamical parameters. In Section 3 we present our results for the simplest dynamical model of a molecule, i.e. one in which the potentials of the two atomic centers are described by (generally, non-equivalent) zero-range (or $\delta$-function) potentials [48]. In Section 3.1 we describe this molecular model system briefly, and present explicit expressions for the dynamical parameters appearing in our general parametrization in Section 2. We then give detailed discussions of interference phenomena and dichroic effects in the photoelectron angular distributions for both symmetric (Section 3.2) and asymmetric (Section 3.3) molecular systems in an elliptically polarized field. We also present the dependence of these angular distributions on both the interatomic distance $R$ and on the orientation of the molecular axis with respect to the polarization plane. For all cases, numerical ZRP results for the angular distributions are also presented. In Section 4 we summarize our results and present some

conclusions. Finally, in Appendix 1 we present some details of the analytic evaluation of the photodetachment amplitudes for our ZRP molecular model. Throughout this manuscript we employ atomic units ($m_e = e = \hbar = 1$).

## 2. Phenomenological parametrization of the molecular photodetachment cross section in an elliptically polarized field

We consider here a very general model of a diatomic molecule comprised of an electron in the field of two attractive potentials separated by the vector $\boldsymbol{R}$, which is a parameter of the problem, without specification of any explicit form for the potentials. For simplicity, we only consider molecules in which the electron is in a $\Sigma$ orbital. Within the electric dipole approximation, the one-photon detachment cross section for this case is determined by the scalar amplitude $A$:

$$\frac{\mathrm{d}\sigma}{\mathrm{d}\Omega} = \frac{4\pi^2 p}{c\omega}|A|^2, \tag{1}$$

$$A = \left\langle \psi_{\boldsymbol{p}}^{(-)} \middle| (\boldsymbol{e}\cdot\hat{\boldsymbol{p}}) \middle| \psi_b \right\rangle, \tag{2}$$

where $\psi_{\boldsymbol{p}}^{(-)}$ is a continuum state with asymptotic ingoing spherical waves, $\psi_b$ is the initial bound state with energy $E_b$, $\omega$ is the frequency of the laser field (so that $p^2/2 = E_b + \omega$), and $\boldsymbol{e}$ is its polarization vector. For the general case of an elliptic polarization, we parameterize the complex polarization vector $\boldsymbol{e}$ ($\boldsymbol{e}\cdot\boldsymbol{e}^* = 1$) in the form:

$$\boldsymbol{e} = \frac{\hat{\boldsymbol{\epsilon}} + i\eta[\hat{\boldsymbol{\kappa}}\times\hat{\boldsymbol{\epsilon}}]}{\sqrt{1+\eta^2}}, \quad -1 \le \eta \le 1, \tag{3}$$

where $\eta$ is the ellipticity of the field, and the unit vectors $\hat{\boldsymbol{\epsilon}}$ and $\hat{\boldsymbol{\kappa}}\times\hat{\boldsymbol{\epsilon}}$ are the directions of the major and minor axes of the polarization ellipse, where $\hat{\boldsymbol{\kappa}}$ is the propagation direction of the laser field. The amplitude $A$ depends linearly on the polarization vector $\boldsymbol{e}$ and must be a scalar. Thus its general form in terms of the other vectors of the problem, $\boldsymbol{R}$ and $\boldsymbol{p}$, can be presented as a superposition of two terms:

$$A = A_p(\boldsymbol{e}\cdot\boldsymbol{p}) + A_R(\boldsymbol{e}\cdot\boldsymbol{R}), \tag{4}$$

where the polarization-independent parameters $A_p \equiv A_p(\omega, \boldsymbol{R}, \boldsymbol{p})$ and $A_R \equiv A_R(\omega, \boldsymbol{R}, \boldsymbol{p})$ depend on the photon energy and on scalar products of the vectors $\boldsymbol{R}$ and $\boldsymbol{p}$. Therefore these parameters are unchanged upon substituting $\boldsymbol{R} \to -\boldsymbol{R}$ and $\boldsymbol{p} \to -\boldsymbol{p}$.

Substituting (4) into (1), we obtain the following general form for the differential cross section:

$$\begin{aligned}\frac{\mathrm{d}\sigma}{\mathrm{d}\Omega} = \frac{4\pi^2 p}{c\omega}\Big[&|A_p|^2|\boldsymbol{e}\cdot\boldsymbol{p}|^2 + |A_R|^2|\boldsymbol{e}\cdot\boldsymbol{R}|^2 \\ &+ 2\mathrm{Re}\left[A_p^* A_R\right]\mathrm{Re}\left[(\boldsymbol{e}^*\cdot\boldsymbol{p})(\boldsymbol{e}\cdot\boldsymbol{R})\right] \\ &- 2\mathrm{Im}\left[A_p^* A_R\right]\mathrm{Im}\left[(\boldsymbol{e}^*\cdot\boldsymbol{p})(\boldsymbol{e}\cdot\boldsymbol{R})\right]\Big].\end{aligned} \tag{5}$$

The scalar products in (5) can be expressed in terms of the linear ($\ell$) and circular ($\xi$) polarization degrees of the photon (which satisfy $\ell^2 + \xi^2 = 1$):

$$\ell = \frac{1-\eta^2}{1+\eta^2} = \boldsymbol{e}\cdot\boldsymbol{e} = \boldsymbol{e}^*\cdot\boldsymbol{e}^*, \quad \xi = \frac{2\eta}{1+\eta^2} = i\hat{\boldsymbol{\kappa}}\cdot[\boldsymbol{e}^*\times\boldsymbol{e}]. \tag{6}$$

Using Equations (3) and (6), we can re-write three of the polarization factors in (5) as:

$$|\boldsymbol{e}\cdot\boldsymbol{p}|^2 = \ell(\hat{\boldsymbol{\epsilon}}\cdot\boldsymbol{p})^2 + \frac{1-\ell}{2}[\hat{\boldsymbol{\kappa}}\times\boldsymbol{p}]^2, \tag{7a}$$

$$\begin{aligned}&\mathrm{Re}\{(\boldsymbol{e}^*\cdot\boldsymbol{p})(\boldsymbol{e}\cdot\boldsymbol{R})\} \\ &\quad = \ell(\hat{\boldsymbol{\epsilon}}\cdot\boldsymbol{p})(\hat{\boldsymbol{\epsilon}}\cdot\boldsymbol{R}) + \frac{1-\ell}{2}[\hat{\boldsymbol{\kappa}}\times\boldsymbol{p}]\cdot[\hat{\boldsymbol{\kappa}}\times\boldsymbol{R}],\end{aligned} \tag{7b}$$

$$\mathrm{Im}\{(\boldsymbol{e}^*\cdot\boldsymbol{p})(\boldsymbol{e}\cdot\boldsymbol{R})\} = \frac{1}{2}\xi(\hat{\boldsymbol{\kappa}}\cdot[\boldsymbol{p}\times\boldsymbol{R}]). \tag{7c}$$

Equation (7c) shows that the last term in (5) differs for $\xi = \pm|\xi|$, and thus describes a circular dichroism effect (i.e. the difference between the angular distributions of photoelectrons for opposite helicities of the elliptically polarized photon). This dichroism effect originates from the interference between the real and imaginary parts of the parameters $A_p$ and $A_R$ [50].

An alternative parametrization of the differential cross section (1) can now be obtained by introducing the cross sections for linearly polarized fields along the major and minor axes of the actual laser field [44]. Indeed, introducing the unit vector $\hat{\boldsymbol{\varepsilon}} \equiv [\hat{\boldsymbol{\epsilon}}\times\hat{\boldsymbol{\kappa}}]$ for the direction of the minor axis of the polarization ellipse and using Equations (5) and (7), the photodetachment cross section can be presented as:

$$\frac{\mathrm{d}\sigma}{\mathrm{d}\Omega} = \frac{1+\ell}{2}\frac{\mathrm{d}\sigma_{\mathrm{lin}}^{(\hat{\boldsymbol{\epsilon}})}}{\mathrm{d}\Omega} + \frac{1-\ell}{2}\frac{\mathrm{d}\sigma_{\mathrm{lin}}^{(\hat{\boldsymbol{\varepsilon}})}}{\mathrm{d}\Omega} + \xi\frac{\mathrm{d}\sigma_{\mathrm{CD}}}{\mathrm{d}\Omega}, \tag{8}$$

where the differential photodetachment cross section $\mathrm{d}\sigma_{\mathrm{lin}}^{(\boldsymbol{n})}/\mathrm{d}\Omega$ for a linearly polarized field with polarization vector $\boldsymbol{n}$ follows from (5) upon making the substitution $\boldsymbol{e} = \boldsymbol{n}$,

$$\begin{aligned}\frac{\mathrm{d}\sigma_{\mathrm{lin}}^{(\boldsymbol{n})}}{\mathrm{d}\Omega} = \frac{4\pi^2 p}{c\omega}\Big\{&|A_p|^2(\boldsymbol{n}\cdot\boldsymbol{p})^2 + |A_R|^2(\boldsymbol{n}\cdot\boldsymbol{R})^2 \\ &+ 2\mathrm{Re}\left[A_p^* A_R\right](\boldsymbol{n}\cdot\boldsymbol{p})(\boldsymbol{n}\cdot\boldsymbol{R})\Big\},\end{aligned} \tag{9}$$

and the explicit form for the dichroic cross section $\mathrm{d}\sigma_{\mathrm{CD}}/\mathrm{d}\Omega$ follows from Equations (5) and (7c):

$$\frac{\mathrm{d}\sigma_{\mathrm{CD}}}{\mathrm{d}\Omega} = \frac{4\pi^2 p}{c\omega}\mathrm{Im}\left[A_p A_R^*\right](\hat{\boldsymbol{\kappa}}\cdot[\boldsymbol{p}\times\boldsymbol{R}]). \tag{10}$$

Note that the general parametrization of the one-photon ionization cross section in [44] was presented in a slightly different (but equivalent) form from that in (8) (see Equation (19) in [44]):

$$\frac{\mathrm{d}\sigma}{\mathrm{d}\Omega} = \frac{\mathrm{d}\sigma_0}{\mathrm{d}\Omega} + \ell\frac{\mathrm{d}\sigma_l}{\mathrm{d}\Omega} + \xi\frac{\mathrm{d}\sigma_{\mathrm{CD}}}{\mathrm{d}\Omega}, \tag{11}$$

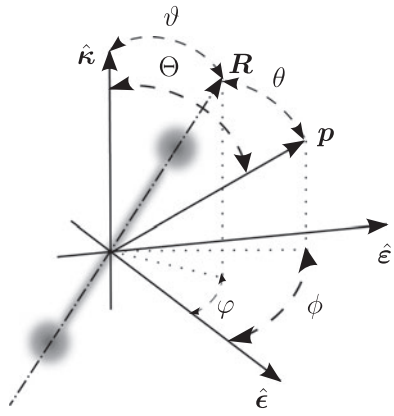


Figure 1. Geometry for the description of one-photon ionization/detachment of a fixed-in-space molecule by an elliptically polarized field.

where

$$\frac{\mathrm{d}\sigma_0}{\mathrm{d}\Omega} = \frac{1}{2}\left(\frac{\mathrm{d}\sigma_{\mathrm{lin}}^{(\hat{\boldsymbol{\epsilon}})}}{\mathrm{d}\Omega} + \frac{\mathrm{d}\sigma_{\mathrm{lin}}^{(\hat{\boldsymbol{\varepsilon}})}}{\mathrm{d}\Omega}\right),$$
$$\frac{\mathrm{d}\sigma_l}{\mathrm{d}\Omega} = \frac{1}{2}\left(\frac{\mathrm{d}\sigma_{\mathrm{lin}}^{(\hat{\boldsymbol{\epsilon}})}}{\mathrm{d}\Omega} - \frac{\mathrm{d}\sigma_{\mathrm{lin}}^{(\hat{\boldsymbol{\varepsilon}})}}{\mathrm{d}\Omega}\right).$$

These general results for the photoelectron angular distribution simplify in particular cases. For the "perpendicular" geometry (in which the molecular axis $\boldsymbol{R}$ is perpendicular to the polarization plane), we have $(\hat{\boldsymbol{\epsilon}}\cdot\boldsymbol{R}) = 0$, $(\hat{\boldsymbol{\varepsilon}}\cdot\boldsymbol{R}) = 0$, and $(\hat{\boldsymbol{\kappa}}\cdot[\boldsymbol{p}\times\boldsymbol{R}]) = 0$, so that the angular distribution is described by only a single invariant parameter:

$$\frac{\mathrm{d}\sigma}{\mathrm{d}\Omega} = \frac{2\pi^2 p^3}{c\omega}|A_p|^2\sin^2\theta(1+\ell\cos 2\phi), \qquad (12)$$

where $\theta$ is the angle between $\boldsymbol{R}$ and $\boldsymbol{p}$, and $\phi$ is the angle between $\hat{\boldsymbol{\epsilon}}$ and the projection of $\boldsymbol{p}$ onto the polarization plane (see Figure 1). (Note that in the perpendicular geometry, $\theta = \Theta$.) The angular distribution also has a simple form if both $\boldsymbol{R}$ and $\boldsymbol{p}$ lie in the polarization plane of a circularly polarized field (i.e. $\xi = \pm 1$):

$$\frac{\mathrm{d}\sigma}{\mathrm{d}\Omega} = \frac{2\pi^2 p}{c\omega}\left\{|A_p|^2 p^2 + |A_R|^2 R^2 + 2\mathrm{Re}\left[A_p^* A_R e^{-i\xi\theta}\right]\right\}. \qquad (13)$$

The dichroic term $\mathrm{d}\sigma_{\mathrm{CD}}/\mathrm{d}\Omega$ in Equation (8) causes a difference in the photodetachment cross sections for elliptically polarized fields with opposite handedness, $\xi = \pm|\xi|$:

$$\Delta_{CD} = \frac{\mathrm{d}\sigma(\xi)}{\mathrm{d}\Omega} - \frac{\mathrm{d}\sigma(-\xi)}{\mathrm{d}\Omega} = \xi\frac{8\pi^2 p}{c\omega}\mathrm{Im}\,[A_p A_R^*](\hat{\boldsymbol{\kappa}}\cdot[\boldsymbol{p}\times\boldsymbol{R}]). \qquad (14)$$

This difference is largest for circularly polarized fields and for a geometry in which both the momentum $\boldsymbol{p}$ of the detached electron and the molecular axis $\boldsymbol{R}$ lie in the polarization plane. It should be emphasized that the dynamic part of the dichroic term is given by the imaginary part of the product $A_p$ and $A_R^*$, so that the dichroism effect disappears in the plane-wave approximation (when the final continuum state $\left|\psi_{\boldsymbol{p}}^{(-)}\right\rangle$ is approximated by a plane wave). Indeed, in the plane-wave approximation, the transition matrix element (2) is Hermitian and the product $A_p A_R^*$ is real. The dichroism term also disappears either upon integration over all directions of the vector $\boldsymbol{p}$ or over all directions of the vector $\boldsymbol{R}$ (i.e. for randomly-oriented molecules).

Since the dichroic term (10) disappears after integration over all directions of the momentum $\boldsymbol{p}$ of the detached electron, the total photodetachment cross section (8) for an elliptically polarized field can be expressed in terms of the total detachment cross sections for two orthogonal linear polarizations:

$$\sigma = \frac{1+\ell}{2}\sigma_{\mathrm{lin}}^{(\hat{\boldsymbol{\epsilon}})} + \frac{1-\ell}{2}\sigma_{\mathrm{lin}}^{(\hat{\boldsymbol{\varepsilon}})}. \qquad (15)$$

The angle-integrated cross section $\sigma_{\mathrm{lin}}^{(\boldsymbol{n})}$ can be parameterized in terms of components perpendicular ($\sigma_\perp$) and parallel ($\sigma_{||}$) to the molecular axis $\boldsymbol{R}$ [40]:

$$\sigma_{\mathrm{lin}}^{(\boldsymbol{n})} = \sigma_\perp + (\sigma_{||} - \sigma_\perp)\left(\boldsymbol{n}\cdot\hat{\boldsymbol{R}}\right)^2, \quad \hat{\boldsymbol{R}} = \boldsymbol{R}/R. \qquad (16)$$

Thus only two independent dynamical parameters are needed for a complete description of the angle-integrated detachment cross section for the case of an elliptically polarized field, while four dynamical parameters are required for the description of the angle-resolved cross section in Equation (5). The total cross section (15) can also be parameterized in terms of $\sigma_\perp$ and $\sigma_{||}$ by introducing the angles $\alpha$ and $\beta$, where $\cos\alpha \equiv \hat{\boldsymbol{\epsilon}}\cdot\hat{\boldsymbol{R}}$ and $\cos\beta \equiv \hat{\boldsymbol{\varepsilon}}\cdot\hat{\boldsymbol{R}}$:

$$\sigma = \frac{1+\ell}{2}\left(\sigma_{||}\cos^2\alpha + \sigma_\perp\sin^2\alpha\right) + \frac{1-\ell}{2}\left(\sigma_{||}\cos^2\beta + \sigma_\perp\sin^2\beta\right). \qquad (17)$$

## 3. Photodetachment of a diatomic molecule in the ZRP molecular model

### 3.1. Field-free molecular model

In order to specify the dynamical parameters $A_p$ and $A_R$ introduced in our phenomenological analysis above, we use a model of a one-electron molecular system comprised of an electron in the field of two attractive ZRPs separated by the distance $R$ (or the vector $\boldsymbol{R}$). Since details of this model have been discussed recently in [48], here we briefly discuss only its main ingredients. Each isolated zero-range (or $\delta$-function) potential supports a single bound $s$ state, $\psi_{E_j^{(0)}}(\boldsymbol{r}) = \sqrt{\kappa_j/(2\pi)}r^{-1}\exp(-\kappa_j r)$, with energy $E_j^{(0)} = -\kappa_j^2/2$ ($j = 1, 2$), where $\kappa_j$ (for definiteness, we assume $\kappa_1 \geq \kappa_2$) is a positive parameter and $\kappa_j^{-1}$ is the scattering length for electron scattering by the $j$th $\delta$-center.

For $R > 1/\sqrt{\kappa_1\kappa_2}$, an electron in the field of two $\delta$-centers localized at positions $\boldsymbol{r} = \boldsymbol{R}_1 = \boldsymbol{R}/2$ and $\boldsymbol{r} = \boldsymbol{R}_2 = -\boldsymbol{R}/2$ has two bound states with energies $E_\pm$: the ground state, $\psi_+(\boldsymbol{r})$, and the excited state, $\psi_-(\boldsymbol{r})$. The corresponding wave functions can be represented as a superposition of two single-ZRP orbitals [48,51]:

$$\psi_\pm(\boldsymbol{r}) = c_1^{(\pm)}\frac{e^{-k_\pm|\boldsymbol{r}-\boldsymbol{R}_1|}}{|\boldsymbol{r}-\boldsymbol{R}_1|} + c_2^{(\pm)}\frac{e^{-k_\pm|\boldsymbol{r}-\boldsymbol{R}_2|}}{|\boldsymbol{r}-\boldsymbol{R}_2|}, \quad k_\pm = \sqrt{-2E_\pm}, \tag{18}$$

where the coefficients $c_1^{(\pm)}$ and $c_2^{(\pm)}$ are:

$$c_1^{(\pm)} = \sqrt{\frac{N_\pm}{4\pi}}\left[1 \pm \frac{\rho_\pm}{\sqrt{1+\rho_\pm^2}}\right]^{1/2},$$
$$c_2^{(\pm)} = \pm\sqrt{\frac{N_\pm}{4\pi}}\left[1 \mp \frac{\rho_\pm}{\sqrt{1+\rho_\pm^2}}\right]^{1/2},$$
$$N_\pm = \frac{k_\pm\sqrt{1+\rho_\pm^2}}{\sqrt{1+\rho_\pm^2} \pm e^{-k_\pm R}}, \quad \rho_\pm = \kappa_- R\, e^{k_\pm R}. \tag{19}$$

The energies $E_+$ and $E_-$ can be found as the solutions of the transcendental equations:

$$k_\pm - \kappa_+ = \pm\sqrt{\kappa_-^2 + \frac{e^{-2k_\pm R}}{R^2}}, \tag{20}$$

where $\kappa_\pm \equiv (\kappa_1 \pm \kappa_2)/2$. Note that $c_1^{(+)} = c_2^{(+)}$ for equivalent $\delta$-centers (for which $\kappa_- = 0$), so that the ground state wave function $\psi_{E_+}(\boldsymbol{r})$ is symmetric with respect to the permutation of $\delta$-centers ($\boldsymbol{R}_1 \leftrightarrows \boldsymbol{R}_2$), while $c_1^{(-)} = -c_2^{(-)}$ and the wave function $\psi_{E_-}(\boldsymbol{r})$ of the excited state is antisymmetric. On the contrary, for nonequivalent centers ($\kappa_- \neq 0$), the major contribution to the wave function (18) comes from one center, while the contribution of the second center decreases exponentially with increasing $R$.

For our molecular model, the continuum (scattering) state of an electron with asymptotic momentum $\boldsymbol{p}$, energy $E = p^2/2$, and satisfying ingoing spherical wave boundary conditions asymptotically can be presented in the form [48,51]:

$$(2\pi)^{3/2}\psi_{\boldsymbol{p}}^{(-)}(\boldsymbol{r}) = e^{i\,\boldsymbol{p}\cdot\boldsymbol{r}} - \frac{1}{\Delta^*(p)}\left[\left((\kappa_2 - ip)e^{i\,\boldsymbol{p}\cdot\boldsymbol{R}_1} - \frac{e^{i\,\boldsymbol{p}\cdot\boldsymbol{R}_2 - ipR}}{R}\right)\frac{e^{-ip|\boldsymbol{r}-\boldsymbol{R}_1|}}{|\boldsymbol{r}-\boldsymbol{R}_1|} + \left((\kappa_1 - ip)e^{i\,\boldsymbol{p}\cdot\boldsymbol{R}_2} - \frac{e^{i\,\boldsymbol{p}\cdot\boldsymbol{R}_1 - ipR}}{R}\right)\frac{e^{-ip|\boldsymbol{r}-\boldsymbol{R}_2|}}{|\boldsymbol{r}-\boldsymbol{R}_2|}\right], \tag{21}$$

where

$$\Delta(p) = (\kappa_1 + ip)(\kappa_2 + ip) - e^{2ipR}/R^2. \tag{22}$$

Further discussion of Equations (18)–(22) can be found in [48].

### 3.2. One-photon detachment of a symmetric molecular system

We begin our analysis with the simplest case: two equivalent centers (i.e. $\kappa_1 = \kappa_2 = \kappa$), which models a symmetric diatomic molecular system. As the analytic evaluation of the photodetachment amplitude (2) in Appendix 1 shows, the results for the dynamical parameters $A_p$ and $A_R$ in Equation (4) for the case of equivalent centers can be presented in the form:

$$A_p = \frac{i^j}{\pi\omega}\sqrt{\frac{N_\pm}{2}}\cos\left(\frac{\boldsymbol{p}\cdot\boldsymbol{R}}{2} + j\frac{\pi}{2}\right), \tag{23a}$$

$$A_R = \frac{i^j}{\pi\omega}\sqrt{\frac{N_\pm}{2}}\sin\left(\frac{\boldsymbol{p}\cdot\boldsymbol{R}}{2} - j\frac{\pi}{2}\right)\mathcal{G}_\pm(p), \tag{23b}$$

$$\mathcal{G}_\pm(p) = \frac{g(p)}{\kappa + ip \mp e^{ipR}/R},$$
$$g(p) = \frac{1}{R}\frac{\partial}{\partial R}\frac{e^{ipR} - e^{-k_\pm R}}{R}. \tag{24}$$

where $j = 0$ and the symbol "+" label the symmetric ground state, while $j = 1$ and the symbol "−" label the antisymmetric excited state.

Explicit expressions for the scalar dynamical amplitudes $A_p$ and $A_R$ show that the imaginary part of the product $A_p^* A_R$ describing the circular dichroism effect is determined by that of the function $\mathcal{G}_\pm(p)$:

$$\mathrm{Im}\,(A_p^* A_R) = \frac{N_\pm}{4(\pi\omega)^2}\sin(\boldsymbol{p}\cdot\boldsymbol{R})\mathrm{Im}\,\mathcal{G}_\pm(p). \tag{25}$$

We emphasize that the interference term in the photodetachment cross section describing dichroic effects disappears for the perpendicular geometry ($\boldsymbol{p} \perp \boldsymbol{R}$), as well as for $\boldsymbol{p}\cdot\boldsymbol{R} = \pi n$ ($n = 1, 2, \ldots$).

The function $\mathcal{G}_\pm(p)$ simplifies for large $R$, in which case it can be approximated as:

$$\mathcal{G}_\pm(p) \approx \frac{ip}{\kappa + ip}\frac{e^{ipR}}{R^2} = \frac{p}{R^2\sqrt{\kappa^2 + p^2}}e^{ipR + i\delta + i\pi/2}, \tag{26}$$

where $\delta$ (defined by $\tan\delta \equiv -p/\kappa$) is the $s$-wave electron scattering phase for a single ZRP and $1/\sqrt{\kappa^2 + p^2}$ is the modulus of the electron scattering amplitude, $f(p)$, for a ZRP: $f(p) = (\kappa + ip)^{-1}$. Substituting (26) into (25), we obtain:

$$\mathrm{Im}\,(A_p^* A_R) = \frac{N_\pm p\sin(\boldsymbol{p}\cdot\boldsymbol{R})\cos(pR + \delta)}{4(\pi\omega R)^2\sqrt{\kappa^2 + p^2}}. \tag{27}$$

For fixed $R$ and large momentum $p$ ($p \gg \kappa$), the interference term (27) simplifies further since $\delta \to -\pi/2$ and $p/\sqrt{\kappa^2 + p^2} \to 1$. Thus, in the limit of large $p$ we obtain:

$$\mathrm{Im}\,(A_p^* A_R) = \frac{N_\pm\sin(\boldsymbol{p}\cdot\boldsymbol{R})\sin(pR)}{4(\pi\omega R)^2}. \tag{28}$$

Although the imaginary part (28) does not decrease with increasing $p$, we note that contribution of the dichroic term in Equation (5) is masked by the leading term $\sim |A_p^{(\pm)}|^2 p^2$

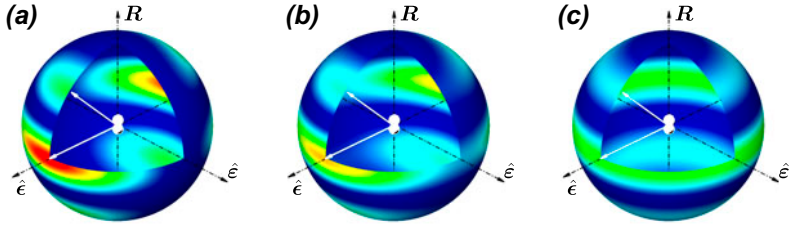


Figure 2. Photoelectron angular distributions for photodetachment by an elliptically polarized laser field with $\omega = 2.56$ a.u. for three values of the ellipticity: (*a*) $\eta = 0$, (*b*) $\eta = 0.5$, and (*c*) $\eta = 1$. The diatomic molecular system in its ground state is oriented perpendicularly to the polarization plane and $\kappa = 1$ a.u., $R = 2$ a.u., and $p = 2$ a.u. The white arrows in the ($\hat{\epsilon}$, $\boldsymbol{R}$) plane mark the positions of the interference maxima corresponding to $\theta = 90°$ and $\theta = 43°$. The sphere shows the surface of $E_p = p^2/2$, while the colors on the sphere indicate the probability of detachment. (The colour version of this figure is included in the online version of the journal.)

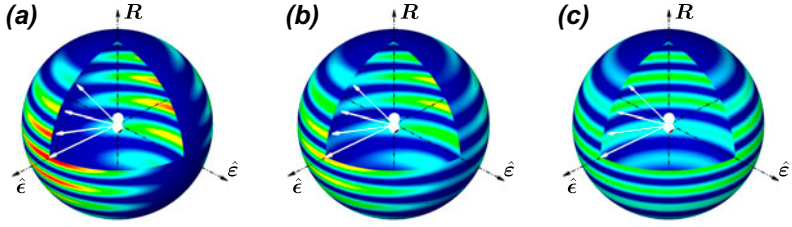


Figure 3. The same as in Figure 2, but for $p = 6$ a.u. (The colour version of this figure is included in the online version of the journal.)

and thus the dichroism effects become weaker with increasing $p$. The dichroic effects disappear also with increasing $R$, since the imaginary part (27) decreases as $R^{-2}$ with increasing $R$.

In Figures 2 and 3 we present 3D photoelectron angular distributions for a symmetric molecular system oriented perpendicularly to the polarization plane of an elliptically polarized field with ellipticity $\eta = 0$, 0.5, and 1. As discussed in Section 2, the dichroic effects vanish in this geometry, while the angular distributions exhibit side lobes, whose number does not depend on the ellipticity. For a linearly polarized field, the side lobes take their maximum values in the plane of the vectors $\hat{\epsilon}$ and $\boldsymbol{R}$, while in the plane of the vectors $\hat{\boldsymbol{\varepsilon}}$ and $\boldsymbol{R}$ the side lobes are vanished (see Figures 2 and 3(*a*)). Indeed, for small ellipticity or for a linearly polarized field, the side lobes are suppressed in the direction of the minor axis of the polarization ellipse owing to the overall factor $(1 + \ell \cos 2\phi)$ (see Equation (12)), which is small for $\phi = \pi/2$ and $3\pi/2$ (and equals zero for $\eta = 0$). With increasing $\eta$, the side lobes form in the plane of the vectors $\hat{\boldsymbol{\varepsilon}}$ and $\boldsymbol{R}$ (see Figures 2 and 3(*b*)) and for circular polarization the formation of side lobes is the same in any plane containing the molecular axis. The intensity of the side lobes gradually decreases from the equatorial plane to the poles in Figures 2 and 3 due to the overall factor $\sin^2\theta$. Note that for the ground state, electron ejection in the direction of the major axis of the polarization ellipse is more probable than in other directions, while for the excited state it is zero. These observations can be explained in terms of two-center interference [11,12]. Indeed, substituting the expression (23a) for $A_p$ into (12) and using the identity $\cos^2(\gamma/2) = (1 + \cos\gamma)/2$ with $\gamma \equiv (\boldsymbol{p}\cdot\boldsymbol{R} + j\pi)$ shows that the two centers of the diatomic molecular system emit two interfering electron waves with phase difference $\boldsymbol{p}\cdot\boldsymbol{R}$ for the ground state and $\boldsymbol{p}\cdot\boldsymbol{R}+\pi$ for the excited state. Each side lobe originates from constructive interference of these two waves and thus in the polarization plane (where $\theta = 90°$ and $\boldsymbol{p}\cdot\boldsymbol{R} = 0$) these two waves interfere constructively for the ground state, but destructively for the excited state. The number of side lobes $N_l$ is given by the number of interference maxima, i.e. $N_l = 2[pR/(2\pi)] + 1$ for the ground state and $N_l = 2[pR/(2\pi)]$ for the excited state. For maxima far from the poles, their positions $\theta_n$ (in terms of the angle $\theta$) can be well approximated by the expression $\theta_n = \arccos[2\pi n/(pR)]$, while near either pole the value of $\theta_n$ is significantly modified by the overall factor $\sin^2\theta$ and thus can be found only numerically.

In Figures 4–6 we present the 2D photodetachment probability distribution as a function of the photoelectron angles $(\Theta, \phi)$ (see Figure 1) for the molecular axis $\boldsymbol{R}$ located in the polarization plane. For the case of linear polarization and the molecular system oriented along the polarization axis, the angular distribution exhibits fourfold symmetry (see Figure 4(*a*)). This symmetry is broken if the angle between the molecular axis and the polarization axis is non-zero (see Figure 4(*b*)). We note that for the angle $\alpha = 90°$ between the molecular axis $\boldsymbol{R}$ and the polarization axis $\hat{\epsilon}$, the angular distribution once again has fourfold symmetry

(see Figure 4(*c*)). This happens for this geometry since $(\boldsymbol{e}\cdot\boldsymbol{R})=0$ and the invariant parameter $A_R$ does not contribute (see Equation (5) and the discussion above for the case of $\boldsymbol{R}$ perpendicular to the polarization plane). Note that different orientations of the molecular axis $\boldsymbol{R}$ with respect to the polarization axis $\hat{\epsilon}$ leads to different interference fringes. Indeed, if the molecular axis is parallel to the polarization axis, the interference fringes have an oval form (see Figure 4(*a*)), while for the perpendicular geometry they have a stripe-like form (see Figure 4(*c*) and compared with Figures 2 and 3(*a*)).

In Figures 5 and 6 we present photoelectron angular distributions for detachment by elliptically- and circularly polarized fields. These angular distributions exhibit noticeable breaking of fourfold symmetry as well as sensitivity to the sign of $\eta$, so that dichroic effects are manifested in these angular distributions. For the molecular system oriented along either the major or minor axes of the polarization ellipse, the angular distributions for opposite signs of $\eta$ have mirror symmetry. This symmetry becomes clear in terms of the parametrization (8). Indeed, the differential cross sections $\mathrm{d}\sigma_{\mathrm{lin}}^{(\hat{\boldsymbol{\epsilon}})}/\mathrm{d}\Omega$ and $\mathrm{d}\sigma_{\mathrm{lin}}^{(\hat{\boldsymbol{\epsilon}})}/\mathrm{d}\Omega$ have fourfold symmetry if the molecular axis is oriented along the major or minor axis of the polarization ellipse (see the discussion above of Figures 4(*a*) and (*c*)), while the CD-term, $\mathrm{d}\sigma_{\mathrm{CD}}/\mathrm{d}\Omega$, changes its sign upon shifting the azimuthal angle $\phi$ by 180° (i.e. $\phi\to\phi+\pi$) (see the definition of the azimuthal angle $\phi$ in Figure 1) for fixed $\xi$. Thus the sign of the CD-term remains unchanged if both $\xi$ and $\varphi$ change sign. This property explains the mirror symmetry in the angular distributions for $\xi\to-\xi$. The angular distribution for a circularly polarized field is fixed by the position of the molecular axis, so that if the molecular axis is shifted by an angle $\Delta\alpha$, then the angular distribution rotates by the same angle (see Figure 6).

Integrated over the solid angle $\Omega_{\boldsymbol{p}}$ of the photoelectron, the photodetachment cross section can be parameterized in terms of parallel ($\sigma_{||}$) and perpendicular ($\sigma_{\perp}$) cross sections (see Equation (15)). For the ZRP molecular model, $\sigma_{\perp}^{(\pm)}$ and $\sigma_{||}^{(\pm)}$ can be expressed in terms of spherical Bessel functions [48]:

$$\sigma_{\perp}^{(\pm)}=\frac{4\pi N_{\pm}p^3}{3c\omega^3}\left[1\pm j_0(x)\pm j_2(x)\right], \tag{29}$$

$$\sigma_{||}^{(\pm)}=\frac{4\pi N_{\pm}p^3}{3c\omega^3}\left[1\pm j_0(x)\mp 2j_2(x)+6\frac{R}{p}\mathrm{Re}\,\mathcal{G}_{\pm}j_1(x)+3\frac{R^2}{p^2}|\mathcal{G}_{\pm}|^2(1\mp j_0(x))\right], \tag{30}$$

where $j_n(x)$ is the spherical Bessel function of the first kind with $x=pR$. If in addition we average over the orientation of the molecular axis, the photodetachment cross section becomes independent of the photon polarization:

$$\overline{\sigma^{(\pm)}}=\frac{1}{3}\sigma_{||}^{(\pm)}+\frac{2}{3}\sigma_{\perp}^{(\pm)}. \tag{31}$$

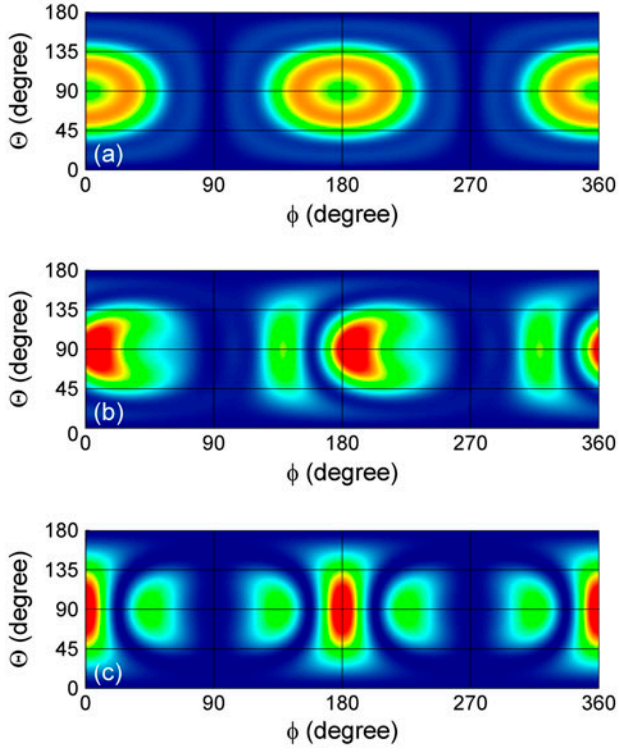


Figure 4. 2D photodetachment probability distribution for the case of linear polarization as a function of the photoelectron angles $(\Theta,\phi)$ (see Figure 1) with the molecular system in its ground state and its axis $\boldsymbol{R}$ located in the polarization plane. Results are shown for three angles $\alpha$ of $\boldsymbol{R}$ relative to the polarization axis $\hat{\epsilon}$: (*a*) $\alpha=0°$; (*b*) $\alpha=45°$; and (*c*) $\alpha=90°$. The molecular system is characterized by its interatomic separation $R=2$ a.u. and $\kappa=1$, and the photon energy is $\omega=2.56$ a.u. (so that $p=2$ a.u.). (The colour version of this figure is included in the online version of the journal.)

If the angular distribution is averaged over the orientation of the molecular axis, the differential cross section takes the simplified form:

$$\overline{\frac{\mathrm{d}\sigma^{(\pm)}}{\mathrm{d}\Omega}}=\frac{\overline{\sigma^{(\pm)}}}{4\pi}\left(1+\beta\frac{3|\boldsymbol{e}\cdot\hat{\boldsymbol{p}}|^2-1}{2}\right) \tag{32}$$

where $\hat{\boldsymbol{p}}=\boldsymbol{p}/p$ and

$$\beta=2\left(1-\frac{\overline{\Delta\sigma^{(\pm)}}}{\overline{\sigma^{(\pm)}}}\right),\quad \overline{\Delta\sigma^{(\pm)}}=\frac{R^2|\mathcal{G}_{\pm}|^2\sigma_{\perp}^{(\pm)}}{p^2}.$$

Integration of $\overline{\frac{\mathrm{d}\sigma^{(\pm)}}{\mathrm{d}\Omega}}$ over the solid angle $\hat{\boldsymbol{p}}$ removes the last term in Equation (32), so that the angle-integrated cross section, $\overline{\sigma^{(\pm)}}$, coincides with Equation (31). Note that the factor $\overline{\Delta\sigma^{(\pm)}}$ behaves asymptotically for large interatomic separations as $\sim R^{-2}$ (and for large $p$ as $\sim p^{-2}$). Thus the angular distribution of photoelectrons for large interatomic separation of a diatomic molecular system approaches that for the atomic ZRP case [50].

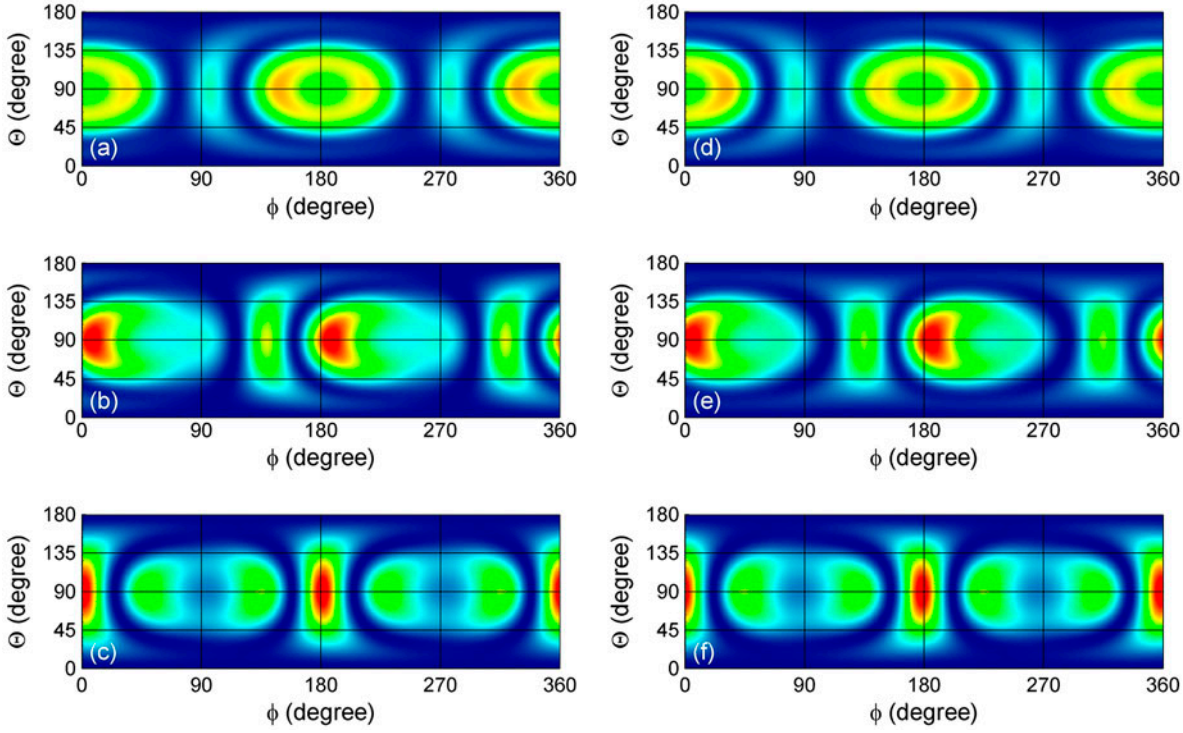


Figure 5. The same as in Figure 4, but for the case of elliptical polarization with $\eta = 0.5$ in panels (*a*)–(*c*) and $\eta = -0.5$ in panels (*d*)–(*f*). (The colour version of this figure is included in the online version of the journal.)

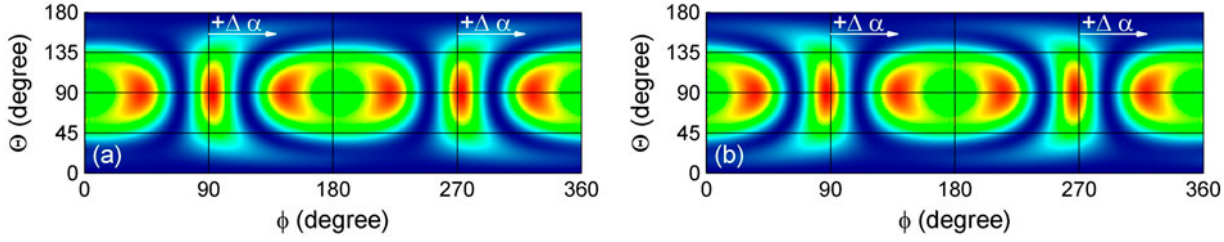


Figure 6. The same as in Figure 5, but for $\eta = 1$ in (*a*) and $\eta = -1$ in (*b*). (The colour version of this figure is included in the online version of the journal.)

### *3.3. One-photon detachment of an asymmetric molecular system*

For the case of an asymmetric molecule, the dynamical parameters $A_p$ and $A_R$ in Equation (4) are more complicated as compared to the symmetric case (see Appendix 1):

$$A_p = \frac{1}{\sqrt{2\pi}\,\omega}\left[c_1^{(\pm)} e^{-i\,\boldsymbol{p}\cdot\boldsymbol{R}/2} + c_2^{(\pm)} e^{i\,\boldsymbol{p}\cdot\boldsymbol{R}/2}\right],$$
$$A_R = \frac{1}{\sqrt{2\pi}\,\omega}\left[b_1(p) e^{-i\,\boldsymbol{p}\cdot\boldsymbol{R}/2} + b_2(p) e^{i\,\boldsymbol{p}\cdot\boldsymbol{R}/2}\right], \quad (33)$$

where

$$b_1(p) = \frac{i}{\Delta}\left[c_2^{(\pm)}(\kappa_2 + ip) + c_1^{(\pm)}\frac{e^{ipR}}{R}\right] g(p),$$
$$b_2(p) = -\frac{i}{\Delta}\left[c_1^{(\pm)}(\kappa_1 + ip) + c_2^{(\pm)}\frac{e^{ipR}}{R}\right] g(p). \quad (34)$$

Since the parameters $A_p$ and $A_R$ are independent of the laser field polarization, they have the same results as were obtained for the case of linear polarization in Ref. [48] (cf. Equation (42) for the one-photon detachment amplitude). The partial amplitude $A_p$ gives the transition matrix element (2) in the plane-wave (or Born) approximation. Two terms in $A_p$ show explicitly the contributions of two centers: an electron can be detached from either of the two atomic centers, whose individual contributions are governed by the magnitudes of the coefficients $c_1^{(\pm)}$ and $c_2^{(\pm)}$. The second partial amplitude, $A_R$, describes a "non-Born" one-photon transition to the spherically outgoing part of the scattering state $\psi_{\boldsymbol{p}}^{(-)}$. This latter amplitude vanishes in the plane-wave approximation.

In order to present the results (33) for $A_p$ and $A_R$ in forms that are more transparent, we consider the limiting case in

which $\rho_\pm \gg 1$ and $pR \gg 1$. In this case, the electron is mostly localized either near the first atomic center (for the case of the ground state $\psi_+$) or near the second atomic center (for the case of the excited state $\psi_-$). For definiteness, we consider the case of the ground state, so that the terms involving $c_2^{(+)}$ can be neglected. In this approximation, the parameters $A_p$ and $A_R$ simplify significantly:

$$A_p \approx \frac{\sqrt{\kappa_1} e^{-i\,\boldsymbol{p}\cdot\boldsymbol{R}/2}}{2\pi\omega},$$
$$A_R \approx \frac{\sqrt{\kappa_1}\, p A_2 e^{i(pR+\delta_2)}}{2\pi\omega R^2}\left[e^{i\,\boldsymbol{p}\cdot\boldsymbol{R}} - A_1 \frac{e^{ipR+i\delta_1}}{R}\right] e^{-i\,\boldsymbol{p}\cdot\boldsymbol{R}/2}, \tag{35}$$

where $A_i = 1/\sqrt{\kappa_i^2 + p^2}$ and $\delta_i$ are, respectively, the modulus of the electron scattering amplitude and the scattering phase ($\tan\delta_i = -p/\kappa_i$) for the $i$th isolated ZRP center. We focus our analysis on the interference term $A_p^* A_R$, since this term contributes most to the asymmetry of the photoelectron angular distributions for nonsymmetric molecules and to the circular dichroism effect. This term originates from the interference of the leading wave, which results from the detachment of the electron from the first atomic center, and the secondary wave, which originates from the scattering of the leading wave from the two atomic centers [9,47]:

$$A_p^* A_R = \frac{\kappa_1 p A_2}{(2\pi\omega R)^2} e^{i(pR + \boldsymbol{p}\cdot\boldsymbol{R} + \delta_2)} - \frac{\kappa_1 p A_2 A_1}{(2\pi\omega R)^2 R} e^{i(2pR+\delta_2+\delta_1)}. \tag{36}$$

The first term in (36) describes the interference between the leading waves emitted from the first center and the secondary wave emitted from the second atomic center (which stems from the scattering of the leading wave from the second center). Indeed, this term is proportional to the electron scattering amplitude $A_2$ from the second center and the corresponding phase difference is given by the quantum mechanical scattering phase, $\delta_2$, and the "geometrical" phase, $pR + \boldsymbol{p}\cdot\boldsymbol{R}$, between the leading and the secondary waves (see Figure 7(a)). The secondary wave emitted from the second center can rescatter from the first center, producing a less intense secondary wave from the first center (see Figure 7(*b*)). The interference between the leading wave and this latter secondary wave is given by the second term in (36). Indeed, this term is proportional to the product $A_2 A_1$ of two scattering amplitudes, which explicitly indicates the double scattering from the first and second atomic centers. The phase of this term equals the sum of the quantum phases, $\delta_2 + \delta_1$, and the "geometrical" phase, $2pR$, which the electron accumulates by moving back and forth between the first and second centers. In contrast to the case of equivalent centers, which are equivalent sources for interfering waves, in the case of nonequivalent centers one center is the source of secondary waves, which interfere with the leading wave produced by the other center. Substituting Equations (35) and (36) into the general Equation (5), we obtain an approximate expression for the photodetachment cross section for large $pR$:

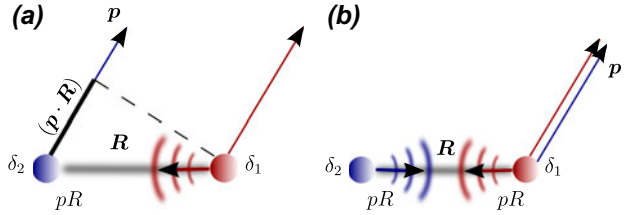


Figure 7. Sketch of different pathways for one-photon detachment from an asymmetric diatomic molecule. (*a*) Right (red) center produces a "leading" wave, which moves to the left (blue) center, which emits secondary waves in the direction of electron detachment. The partial phase shifts accumulated along each step are indicated: the "geometrical" phase between the two centers, $pR$; the quantum mechanical phase, $\delta_2$, resulting from interaction with the left atomic center; and the "geometrical" phase difference, $(\boldsymbol{p}\cdot\boldsymbol{R})$, between the secondary and leading waves in the direction of detachment. (*b*) Right (red) center produces a "leading" wave, which moves to the left (blue) center. The left center is a source of a secondary wave, which moves back to the right center and leads to a reflected wave from the right center that is emitted in the detachment direction. The partial phase shifts accumulated along each step are indicated: the "geometrical" phase between the two centers, $pR$ in each direction; and two quantum mechanical phases, $\delta_1$ and $\delta_2$, resulting from interaction with the two atomic centers. (The colour version of this figure is included in the online version of the journal.)

$$\frac{\mathrm{d}\sigma}{\mathrm{d}\Omega} \approx \sigma_1 \left[\frac{3}{4\pi}|\boldsymbol{e}\cdot\hat{\boldsymbol{p}}|^2 + \frac{3}{2\pi} \times \frac{A_2|(\boldsymbol{e}\cdot\hat{\boldsymbol{p}})(\boldsymbol{e}\cdot\hat{\boldsymbol{R}})|}{R}\cos(pR + \boldsymbol{p}\cdot\boldsymbol{R} + \delta_2 + \Phi)\right],$$
$$\Phi = \tilde{\phi}_R - \tilde{\phi}_p. \tag{37}$$

where $\sigma_1 = (4\pi\kappa_1 p^3)/(3c\omega^3)$, $\tilde{\phi}_p = \arg(\boldsymbol{e}\cdot\boldsymbol{p})$, and $\tilde{\phi}_R = \arg(\boldsymbol{e}\cdot\boldsymbol{R})$. For linear polarization $\Phi = 0$, while for circular polarization $\Phi = -\xi\theta$, where $\theta$ is the angle between $\boldsymbol{p}$ and $\boldsymbol{R}$.

Although the origin of interference fringes is the same for both linear and circular polarization, there is a crucial difference between the photoelectron angular distributions for linear and circular polarizations. In Figures 8–10 we present the angular distribution of electrons detached by linearly polarized and by circularly polarized fields. (For the circularly polarized field, we consider a molecular system oriented in the polarization plane.) Our numerical results show that interference fringes for linear polarization are sensitive to the orientation of the molecular axis with respect to the polarization axis: the interference effects are maximal if the molecular axis is collinear with the polarization axis and they disappear completely if these axes are perpendicular to one another. Moreover, the interference fringes for

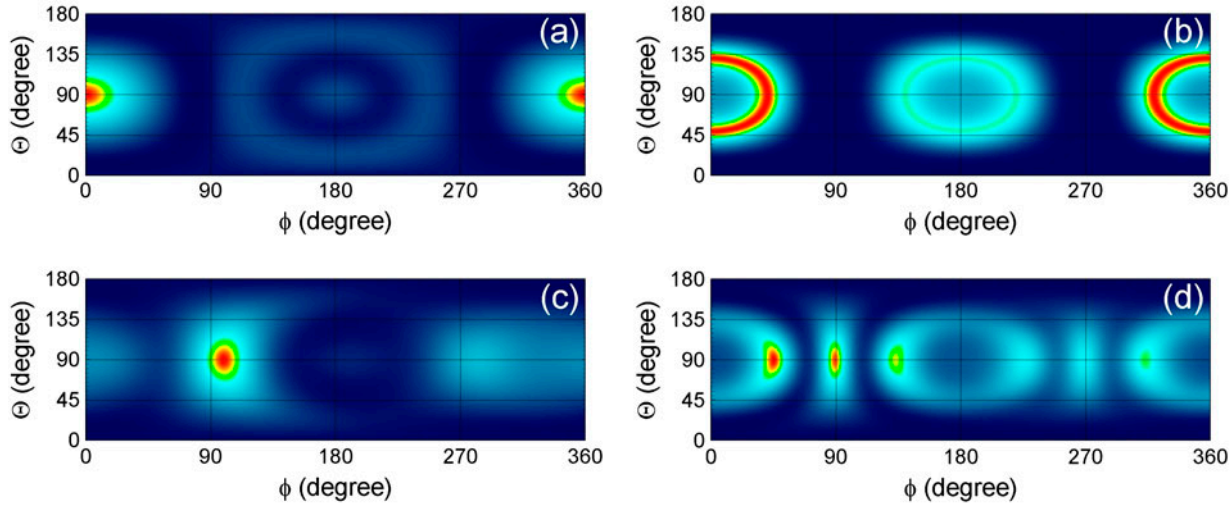


Figure 8. 2D map of the photoelectron angular distribution in photodetachment of an asymmetric molecular system in its ground state ($\kappa_1 = 1$ a.u., $\kappa_2 = 0.8$ a.u., interatomic distance $R = 2$ a.u.) for $\omega = 2$ a.u. (panels (*a*) and (*c*)) and $\omega = 10$ a.u. (panels (*b*) and (*d*)). Results for linear polarization are in the upper row (panels (*a*) and (*b*)), while results for the circular polarization are in the bottom row (panels (*c*) and (*d*)). The molecule is oriented along the major polarization axis. Angles $\Theta$ and $\phi$ are shown in Figure 1. (The colour version of this figure is included in the online version of the journal.)

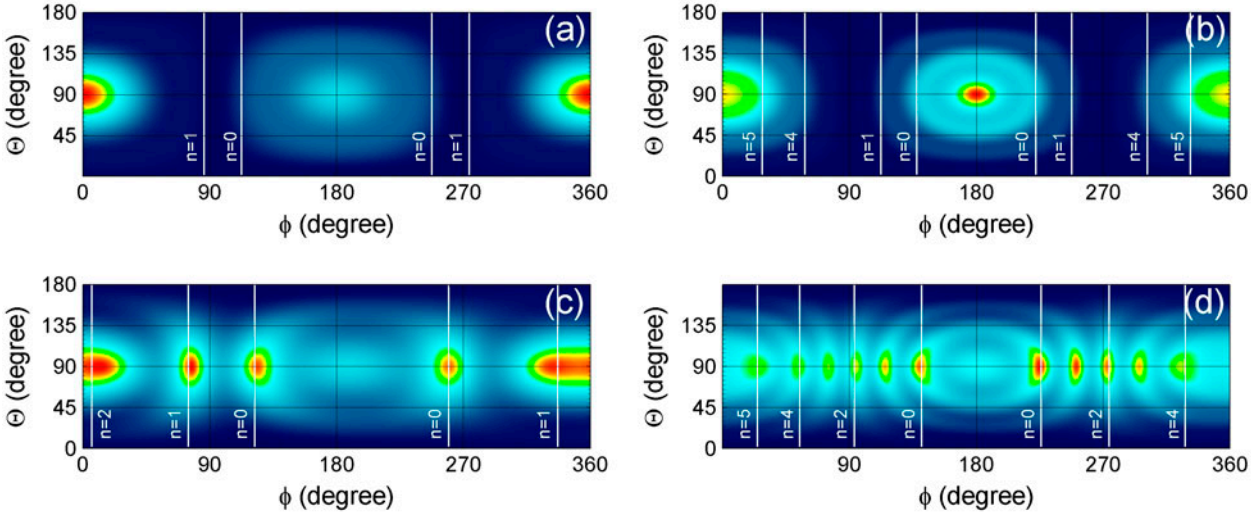


Figure 9. The same as in Figure 8, but for $R = 4$ a.u. Vertical lines mark the positions of maxima given by (38) for given $n$. (The colour version of this figure is included in the online version of the journal.)

a linearly polarized field are masked by the contribution of the leading term (i.e. the first term in (37)), which only disappears for the same geometry as the interference term (i.e. when $(\boldsymbol{e} \cdot \boldsymbol{p}) = 0$). For the case of a circularly polarized field, the interference fringes are pronounced in the polarization plane, and their form does not change upon changing the orientation of the molecular system in the polarization plane. We note, however, that for the case of a circularly polarized field, a rotation of the molecular axis by the angle $\alpha$ leads to a rotation of the angular distribution by the same angle. In contrast to the case of linear polarization, for circular polarization with the electron momentum $\boldsymbol{p}$ in the polarization plane, we have $|\boldsymbol{e} \cdot \hat{\boldsymbol{p}}| = |\boldsymbol{e} \cdot \hat{\boldsymbol{R}}| = 1/\sqrt{2}$, so that the leading and interference terms contribute with the same angle-independent weights.

Interference phenomena in the photodetachment cross section for asymmetric molecules originate from the interference term $A_p^* A_R$, whose approximate expression is given by Equation (36). The positions of the interference maxima and minima for the cases of both linear and circular polarization can be found using Equation (37). (For simplicity, we only consider the case when both vectors $\boldsymbol{p}$ and $\boldsymbol{R}$ lie in the polarization plane.) The positions of the interference maxima for an arbitrary polarization are given by:

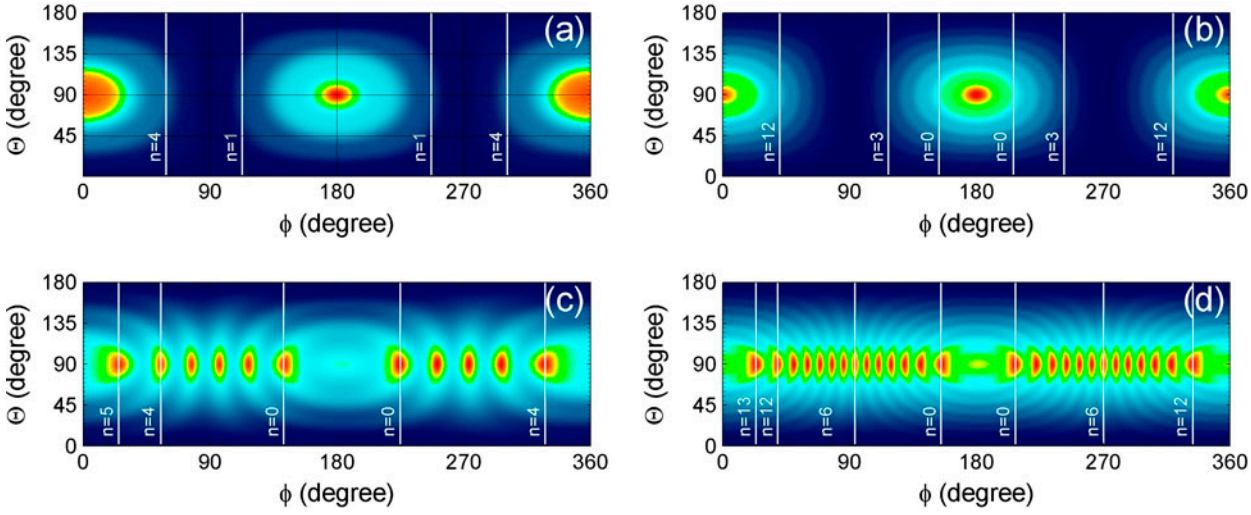


Figure 10. The same as in Figure 9, but for $R = 10$ a.u. (The colour version of this figure is included in the online version of the journal.)

$$2pR\cos^2\theta/2 + \delta_2 - \xi\theta = 2\pi n + \ell\pi\Lambda(\theta), \qquad (38)$$

where $n = 0\cdots[pR/\pi]$ (where the square brackets $[x]$ denote the integer part of $x$), $\theta$ is the angle between $\boldsymbol{p}$ and $\boldsymbol{R}$, and $\Lambda(\theta)$ depends upon the sign of $\boldsymbol{e}\cdot\hat{\boldsymbol{p}}$: $\Lambda(\theta) = 1$ for $\theta \in (\pi/2, 3\pi/2)$ and $\Lambda = 0$ otherwise. We emphasize that Equations (37) and (38) only apply for circularly- and linearly polarized fields, where $\xi = \pm 1$ ($\ell = 0$) for a circularly polarized field and $\xi = 0$ ($\ell = 1$) for a linearly polarized field. Expression (38) is applicable for large $pR$, which is suitable for observation of interference phenomena. For a linearly polarized field, the positions of the maxima are symmetric with respect to $\theta = \pi$, while for a circularly polarized field this symmetry breaks down owing to the dichroic term, $\xi\theta$. It should be emphasized that interference phenomena for the case of linear polarization are suppressed due to the additional modulation factor, $(\boldsymbol{e}\cdot\boldsymbol{p}) \sim \sin\theta$. Thus the observation of interference phenomena is more appropriate for the case of circular polarization.

## 4. Conclusions

In this paper, we have presented an analytic description of one-photon molecular ionization/detachment by an elliptically polarized monochromatic field based on a simple one-electron, two-center molecular model. Our phenomenological analysis shows that the general parametrization of the differential (angle-resolved) photoionization cross section for the case of an elliptically polarized field involves four dynamical parameters, which can be expressed in terms of two polarization-independent complex parameters ($A_p$ and $A_R$) that comprise the photoionization amplitude (see Equations (4) and (5)). One of the four dynamical parameters (i.e. the product $A_p A_R^*$) corresponds to the dichroic term in the cross section, which depends on the helicity of the photon and describes the circular dichroism effects in the photoelectron angular distribution. The general parametrization (5) for the differential cross section simplifies significantly in two particular cases: (i) the perpendicular geometry (in which the molecular axis is perpendicular to the polarization plane, see Equation (12)); and (ii) the polarization plane geometry (in which both the molecular axis and the photoelectron momentum lie in the polarization plane of a circularly polarized field, see Equation (13)).

In order to demonstrate quantitatively the interference and dichroic effects for both symmetric and asymmetric molecular systems, we used the analytic results for the dynamical molecular parameters $A_p$ and $A_R$ obtained for the two ZRP molecular model. Since for this model only two (ground and excited) bound electron states exist, these results can be used for a qualitative description of photodetachment of a negative molecular ion. For a symmetric molecular system, we have shown that two-center interference effects can be observed more easily in the photoelectron angular distributions produced by a circularly polarized field for the perpendicular geometry. (As Figure 3(*c*) shows, the interference fringes for this case have the form of uniform concentric strips around the molecular axis.) However, dichroic effects disappear completely for the case of perpendicular geometry. These effects for the symmetric molecular system have been discussed for a molecule oriented in the plane of the polarization ellipse. The parametrization of the photoelectron angular distribution for a randomly oriented symmetric molecular system can be expressed in terms of total (angle-integrated) detachment cross sections of the molecular system in two linearly polarized fields, whose polarization vectors are, respectively, perpendicular and parallel to the molecular axis (see Equation (32)).

For asymmetric molecules, we have shown that the interference fringes have a different origin from those in the case

of symmetric molecules. For this case, one molecular center produces "direct" electronic waves, while the second center emits a "secondary" wave. Thus the interference fringes are formed as the result of interference between the direct and secondary waves. Our analysis shows that dichroic effects for the case of asymmetric molecules modify the interference patterns by adding extra interference maxima to the angular distribution. For linearly- and circularly polarized fields and large photoelectron momenta, we have derived an analytic expression (38) for the angular locations of the interference maxima in the photoelectron angular distributions.

## Disclosure statement

No potential conflict of interest was reported by the authors.

## Funding

This work was supported in part by RFBR [grant number 13-02-00447]; the Ministry of Education and Science of the Russian Federation under [Project No. 1019]; by NSF [grant number PHY-1208059]; the Dynasty Foundation (M.V.F).

## ORCID

*Anthony F. Starace* http://orcid.org/0000-0001-7261-9329
*M.V. Frolov* http://orcid.org/0000-0001-6651-4619
*N.L. Manakov* http://orcid.org/0000-0001-6134-7276
*S.S. Marmo* http://orcid.org/0000-0002-1534-9526

## References

[1] Corkum, P.; Krausz, F. *Nat. Phys.* **2007,** *3,* 381–387.
[2] Plaja, L.; Torres, R.; Zair, A., Eds. *Attosecond Physics: Attosecond Measurements and Control of Physical Systems*; Springer-Verlag: Berlin, 2013.
[3] Lépine, F.; Ivanov, M.Y.; Vrakking, M.J.J. *Nature Photon.* **2014,** *8,* 195–204.
[4] Schultz, T.; Vrakking, M., Eds. *Attosecond and XUV Physics: Ultrafast Dynamics and Spectroscopy*; Wiley-VCH: Weinheim, 2014.
[5] Pronin, E.A.; Starace, A.F.; Frolov, M.V.; Manakov, N.L. *Phys. Rev. A* **2009,** *80,* 063403.
[6] Hu, S.X.; Collins, L.A.; Schneider, B.I. *Phys. Rev. A* **2009,** *80,* 023426.
[7] Yuan, K.-J.; Lu, H.; Bandrauk, A.D. *Chem. Phys. Chem.* **2013,** *14,* 1496–1501.
[8] Yuan, K.-J.; Bian, X.-B.; Bandrauk, A.D. *Phys. Rev. A* **2014,** *90,* 023407.
[9] Zimmermann, B.; Rolles, D.; Langer, B.; Hentges, R.; Braune, M.; Cvejanovic, S.; Geßner, O.; Heiser, F.; Korica, S.; Lischke, T.; Reinköster, A.; Viefhaus, J.; Dörner, R.; McKoy, V.; Becker, U. *Nat. Phys.* **2008,** *4,* 649–655.
[10] Guan, X.; Secor, E.B.; Bartschat, K.; Schneider, B.I. *Phys. Rev. A* **2012,** *85,* 043419.
[11] Cohen, H.D.; Fano, U. *Phys. Rev.* **1966,** *150,* 30–33.
[12] Kaplan, I.G.; Markin, A.P. *Sov. Phys. Dokl. (Engl. Transl.)* **1969,** *14,* 36; *Dok. Akad. Nauk SSSR* **1969,** *184,* 66–69.
[13] Ilchen, M.; Glaser, L.; Scholz, F.; Walter, P.; Deinert, S.; Rothkirch, A.; Seltmann, J.; Viefhaus, J.; Decleva, P.; Langer, B.; Knie, A.; Ehresmann, A.; Al-Dossary, O.M.; Braune, M.; Hartmann, G.; Meissner, A.; Tribedi, L.C.; AlKhaldi, M.; Becker, U. *Phys. Rev. Lett.* **2014,** *112,* 023001.
[14] Morishita, T.; Le, A.-T.; Chen, Z.; Lin, C.D. *Phys. Rev. Lett.* **2008,** *100,* 013903.
[15] Le, A.-T.; Morishita, T.; Lin, C.D. *Phys. Rev. A* **2008,** *78,* 023814.
[16] Frolov, M.V.; Manakov, N.L.; Sarantseva, T.S.; Emelin, M.Y.; Ryabikin, M.Y.; Starace, A.F. *Phys. Rev. Lett.* **2009,** *102,* 243901.
[17] Zheltukhin, A.N.; Manakov, N.L.; Flegel, A.V.; Frolov, M.V. *J.E.T.P. Lett. (Engl. Transl.)* **2011,** *94,* 599–605; *Zh. Eksp. Teor. Fiz. Pis. Red.* **2011,** *94,* 641–646.
[18] Zheltukhin, A.N.; Flegel, A.V.; Frolov, M.V.; Manakov, N.L.; Starace, A.F. *J. Phys. B* **2012,** *45,* 081001.
[19] Zheltukhin, A.N.; Flegel, A.V.; Frolov, M.V.; Manakov, N.L.; Starace, A.F. *Phys. Rev. A* **2014,** *89,* 023407.
[20] Wörner, H.J.; Niikura, H.; Bertrand, J.B.; Corkum, P.B.; Villeneuve, D.M. *Phys. Rev. Lett.* **2009,** *102,* 103901.
[21] Shiner, A.D.; Schmidt, B.E.; Trallero-Herrero, C.; Wörner, H.J.; Patchkovskii, S.; Corkum, P.B.; Kieffer, J.-C.; Légaré, F.; Villeneuve, D.M. *Nat. Phys.* **2011,** *7,* 464–467.
[22] Lein, M.; Hay, N.; Velotta, R.; Marangos, J.P.; Knight, P.L. *Phys. Rev. Lett.* **2002,** *88,* 183903.
[23] Lein, M.; Hay, N.; Velotta, R.; Marangos, J.P.; Knight, P.L. *Phys. Rev. A* **2002,** *66,* 023805.
[24] Itatani, J.; Levesque, J.; Zeidler, D.; Niikura, H.; Pépin, H.; Kieffer, J.C.; Corkum, P.B.; Villeneuve, D.M. *Nature* **2004,** *432,* 867–871.
[25] Vozzi, C.; Calegari, F.; Benedetti, E.; Caumes, J.-P.; Sansone, G.; Stagira, S.; Nisoli, M.; Torres, R.; Heesel, E.; Kajumba, N.; Marangos, J.P.; Altucci, C.; Velotta, R. *Phys. Rev. Lett.* **2005,** *95,* 153902.
[26] Baker, S.; Robinson, J.S.; Haworth, C.A.; Teng, H.; Smith, R.A.; Chirilă, C.C.; Lein, M.; Tisch, J.W.G.; Marangos, J.P. *Science* **2006,** *312,* 424–427.
[27] Torres, R.; Kajumba, N.; Underwood, J.G.; Robinson, J.S.; Baker, S.; Tisch, J.W.G.; de Nalda, R.; Bryan, W.A.; Velotta, R.; Altucci, C.; Turcu, I.C.E.; Marangos, J.P. *Phys. Rev. Lett.* **2007,** *98,* 203007.
[28] Torres, R.; Siegel, T.; Brugnera, L.; Procino, I.; Underwood, J.G.; Altucci, C.; Velotta, R.; Springate, E.; Froud, C.; Turcu, I.C.E.; Patchkovskii, S.; Ivanov, M.Yu.; Smirnova, O.; Marangos, J.P. *Phys. Rev. A* **2010,** *81,* 051802(R).
[29] Lin, C.D.; Le, A.-T.; Chen, Z.; Morishita, T.; Lucchese, R. *J. Phys. B* **2010,** *43,* 122001.
[30] van der Zwan, E.V.; Lein, M. *Phys. Rev. A* **2010,** *82,* 033405.
[31] Bertrand, J.B.; Wörner, H.J.; Hockett, P.; Villeneuve, D.M.; Corkum, P.B. *Phys. Rev. Lett.* **2012,** *109,* 143001.
[32] Wong, M.C.H.; Le, A.-T.; Alharbi, A.F.; Boguslavskiy, A.E.; Lucchese, R.R.; Brichta, J.-P.; Lin, C.D.; Bhardwaj, V.R. *Phys. Rev. Lett.* **2013,** *110,* 033006.
[33] Smirnova, O.; Mairesse, Y.; Patchkovskii, S.; Dudovich, N.; Villeneuve, D.; Corkum, P.; Ivanov, M. Yu *Nature* **2009,** *460,* 972–977.
[34] Haessler, S.; Caillat, J.; Boutu, W.; Giovanetti-Teixeira, C.; Ruchon, T.; Auguste, T.; Diveki, Z.; Breger, P.; Maquet, A.; Carré, B.; Taieb, R.; Salières, P. *Nat. Phys.* **2010,** *6,* 200–206.
[35] Mairesse, Y.; Higuet, J.; Dudovich, N.; Shafir, D.; Fabre, B.; Mével, E.; Constant, E.; Patchkovskii, S.; Walters, Z.; Ivanov, M.Yu.; Smirnova, O. *Phys. Rev. Lett.* **2010,** *104,* 213601.
[36] Vozzi, C.; Negro, M.; Calegari, F.; Sansone, G.; Nisoli, M.; De Silvestri, S.; Stagira, S. *Nature Phys.* **2011,** *7,* 822–826.
[37] Haessler, S.; Caillat, J.; Salières, P. *J. Phys. B* **2011,** *44,* 203001.

[38] Shafir, D.; Soifer, H.; Bruner, B.D.; Dagan, M.; Mairesse, Y.; Patchkovskii, S.; Ivanov, M.Yu.; Smirnova, O.; Dudovich, N. *Nature* **2012,** *485,* 343–346.
[39] Serbinenko, V.; Smirnova, O. *J. Phys. B* **2013,** *46,* 171001.
[40] Guan, X.; Secor, E.B.; Bartschat, K.; Schneider, B.I. *Phys. Rev. A* **2011,** *84,* 033420.
[41] Miyagi, H.; Morishita, T.; Watanabe, S. *Phys. Rev. A* **2012,** *85,* 022708.
[42] Yuan, K.-J.; Bandrauk, A.D. *Phys. Rev. A* **2012,** *85,* 053419.
[43] Guan, X.; Secor, E.B.; DuToit, R.C.; Bartschat, K. *Phys. Rev. A* **2012,** *86,* 053425.
[44] Guan, X.; DuToit, R.C.; Bartschat, K. *Phys. Rev. A* **2013,** *87,* 053410.
[45] Yuan, K.-J.; Chelkowski, S.; Bandrauk, A.D. *Chem. Phys. Lett.* **2014,** *592,* 334–340.
[46] Yuan, K.-J.; Bandrauk, A.D. *Photonics* **2015,** *2,* 71–92.
[47] Becker, U. *Nature* **2011,** *474,* 586–587.
[48] Borzunov, S.V.; Frolov, M.V.; Ivanov, M.Yu.; Manakov, N.L.; Marmo, S.S.; Starace, A.F. *Phys. Rev. A* **2013,** *88,* 033410.
[49] Baltenkov, A.S.; Becker, U.; Manson, S.T.; Msezane, A.Z. *J. Phys. B* **2012,** *45,* 035202.
[50] Manakov, N.L.; Frolov, M.V.; Borca, B.; Starace, A.F. *J. Phys. B* **2003,** *36,* R49–R124.
[51] Demkov, Y.N.; Ostrovsky, V.N. *Zero-Range Potentials and their Applications in Atomic Physics*; Plenum: New York, 1988.


## Appendix 1.

The analytic evaluation of the photodetachment amplitude (2) for the ZRP molecular model is simplified in the momentum representation. Performing the Fourier transformation of Equations (18) and (21), we obtain the following results for the bound state wave functions $\psi_\pm$ and the continuum state $\psi_{\boldsymbol{p}}^{(-)}$ in the momentum representation:

$$\psi_\pm(\mathbf{q}) = \sqrt{\frac{2}{\pi}}\frac{1}{q^2+k_\pm^2}\left(c_1^\pm e^{-i\mathbf{q}\cdot\boldsymbol{R}_1} + c_2^\pm e^{-i\mathbf{q}\cdot\boldsymbol{R}_2}\right), \tag{A1}$$

$$\begin{aligned}\psi_{\boldsymbol{p}}^{(-)}(\mathbf{q}) = {}& \delta(\mathbf{q}-\boldsymbol{p}) - \frac{1}{2\pi^2(\Delta(p))^*} \\ & \times\left[\left((\kappa_2 - ip)e^{i\boldsymbol{p}\cdot\boldsymbol{R}_1} - \frac{e^{i\boldsymbol{p}\cdot\boldsymbol{R}_2 - ipR}}{R}\right)\frac{e^{-i\mathbf{q}\cdot\boldsymbol{R}_1}}{q^2-p^2+i0}\right. \\ & \left. + \left((\kappa_1 - ip)e^{i\boldsymbol{p}\cdot\boldsymbol{R}_2} - \frac{e^{i\boldsymbol{p}\cdot\boldsymbol{R}_1 - ipR}}{R}\right)\frac{e^{-i\mathbf{q}\cdot\boldsymbol{R}_2}}{q^2-p^2+i0}\right].\end{aligned} \tag{A2}$$

Substituting these expressions into the definition (2) for the photodetachment amplitude $A$ and replacing the operator $\hat{\boldsymbol{p}}$ by the integration variable $\mathbf{q}$, we obtain after some simple algebra:

$$\begin{aligned}A = \sqrt{\frac{2}{\pi}}\Bigg\{ & \frac{1}{p^2+k_\pm^2}\left(c_1^\pm e^{-i\boldsymbol{p}\cdot\boldsymbol{R}/2} + c_2^\pm e^{i\boldsymbol{p}\cdot\boldsymbol{R}/2}\right)(\boldsymbol{e}\cdot\boldsymbol{p}) \\ & - \frac{1}{2\pi^2\Delta}\Bigg[c_1^\pm\left((\kappa_1+ip)e^{i\boldsymbol{p}\cdot\boldsymbol{R}/2} - \frac{e^{ipR}}{R}e^{-i\boldsymbol{p}\cdot\boldsymbol{R}/2}\right)I(\boldsymbol{R}) \\ & + c_2^\pm\left((\kappa_2+ip)e^{-i\boldsymbol{p}\cdot\boldsymbol{R}/2} - \frac{e^{ipR}}{R}e^{i\boldsymbol{p}\cdot\boldsymbol{R}/2}\right)I(-\boldsymbol{R})\Bigg]\Bigg\},\end{aligned} \tag{A3}$$

where

$$\begin{aligned}I(\boldsymbol{R}) &= \int \frac{(\boldsymbol{e}\cdot\mathbf{q})e^{-i\mathbf{q}\cdot\boldsymbol{R}}}{\left(q^2+k_\pm^2\right)\left(q^2-p^2-i0\right)}d\mathbf{q} \\ &= i\left(\boldsymbol{e}\cdot\frac{\partial}{\partial\boldsymbol{R}}\right)\int\frac{e^{-i\mathbf{q}\cdot\boldsymbol{R}}}{\left(q^2+k_\pm^2\right)\left(q^2-p^2-i0\right)}d\mathbf{q}.\end{aligned}$$

Performing the integration in $I(\boldsymbol{R})$ over the angular variables of the vector $\mathbf{q}$ and calculating the final integral over $q$ using the residue theorem, we find

$$I(\boldsymbol{R}) = -I(-\boldsymbol{R}) = i\frac{2\pi^2 g}{p^2+k_\pm^2}(\boldsymbol{e}\cdot\boldsymbol{R}),$$

where

$$g = \frac{1}{R}\frac{\partial}{\partial R}\frac{e^{ipR}-e^{-k_\pm R}}{R}.$$

Substituting these expressions for $I(\pm\boldsymbol{R})$ into (A3), we obtain for the amplitude $A$ the result (4) with the parameters $A_p$ and $A_R$ given by (33). For the case of equivalent centers, $\kappa_1 = \kappa_2 = \kappa$; using Equations (33) for the parameters $A_p$ and $A_R$, we obtain after some algebra the expressions (23a) and (23b).